Passivation-free high performance self-powered photodetector based on Si nanostructure-PEDOT:PSS hybrid heterojunction

Kumaar Swamy Reddy Bapathi [ab], Mostafa F. Abdelbar [cd], Wipakorn Jevasuwan [c], Pramod H Borse [b], Sushmee Badhulika [a] and Naoki Fukata [c]**

[a] *Department of Electrical Engineering, Indian Institute of Technology Hyderabad, Kandi, Sangareddy, Hyderabad*

[b] *Centre for Solar Energy Materials, International Advanced Research Centre for Powder Metallurgy & New Materials, Balapur, Hyderabad*

[c] *Nanostructured Semiconducting Materials Group, Centre for Materials Nanoarchitectonics, National Institute for Materials Science, Tsukuba, Japan*

[d] *Institute of Nanoscience & Nanotechnology, Kafrelsheikh University, 33516 Kafrelsheikh, Egypt*

GRAPHICAL ABSTRACT

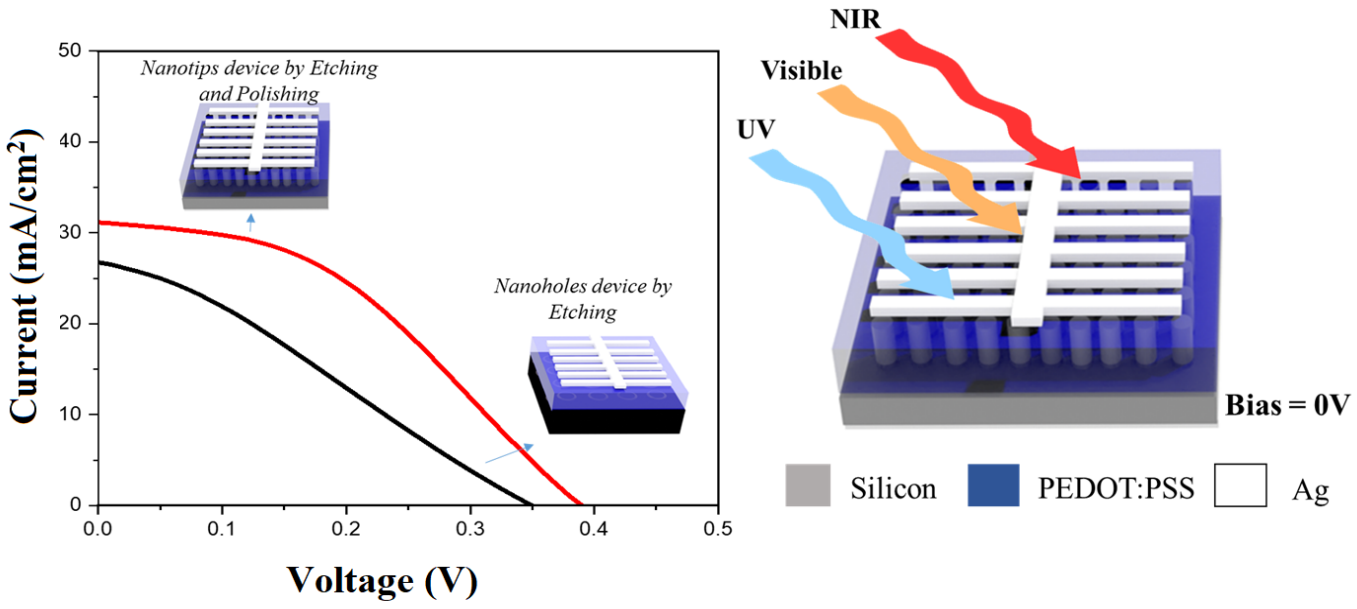

ABSTRACT

Hybrid heterojunction between organic PEDOT:PSS and inorganic Silicon (Si) nanostructures is promising for high-performance self-powered photodetectors due to their favourable band energetics and ease of processing. Traditionally, Si nanostructures require additional passivation layers to reduce surface defect states, which adds complexity and involves the use of harmful organic solvents. Here in, we demonstrate a simple chemical polishing process to reduce defects and fabricate a conformable heterojunction between Si nanostructures and PEDOT:PSS. Si nanostructures fabricated by metal-assisted chemical etching (MACE) technique and subsequently treated by the chemical polishing process are spin-coated with PEDOT:PSS to form heterojunction and employed as self-powered broadband photodetector. The optimized device shows superior performance, such as high responsivity of 555.34 mA/W, quick rise/fall times of 79 ms / 81 ms, high External Quantum Efficiency (EQE) of 0.8 at zero bias (0V) and high photostability up to 500 illumination cycles. Dark I-V characteristics and carrier lifetime measurements reveal that the enhanced performance of chemically polished devices is attributed to the formation of a conformable heterojunction and reduction in defects in the Si nanostructures. Given the scalability and simplicity of the demonstrated passivation-free approach, this work may aid the fabrication of high-performance hybrid Si nanostructured photodetectors.

Keywords: hybrid heterojunction, Silicon nanostructures, PEDOT:PSS, self-powered photodetector, Metal-assisted chemical etching, chemical polishing

1. INTRODUCTION

Self-powered photodetectors, also known as self-driven photodetectors, are devices capable of detecting photons without any external power or bias. These self-powered devices have gained significant research interest in recent years owing to its potential for energy efficient and low-power applications. Self-powered photodetectors find wide range of usage in applications such as wireless sensors, gesture proximity sensing, energy-efficient lighting, security systems, medical devices, consumer electronics and energy harvesting devices etc.[1–4] Self-photodetectors majorly rely on photovoltaic effect to detect the light, where the incoming photons create electron-hole pairs and are separated by built-in electric in the device, giving rise to photocurrent.

Among the various self-powered device architectures, hybrid heterojunctions based on Organic-Inorganic interfaces have garnered significant research attention and have demonstrated potential in fabricating high performance and low-cost devices. Organic materials such as conducting polymers have been extensively employed as charge transport layers in photonic devices. PEDOT:PSS, a p-type conducting polymer, owing to its excellent solution processability and high conductivity is employed as hole transport layer. A heterojunction between the Organic PEDOT: PSS and inorganic silicon (Si) is widely employed for solar cell applications due to their excellent band level offset and Schottky junction characteristics[5–10]. However, despite its potential, the research on Silicon-PEDOT:PSS hybrid junction for photodetection is still limited.

Typically, conventional planar Si based hybrid junction photodetectors, exhibit retarded performance due to the limited interfacial contact area between Si and PEDOT:PSS. Hence, in order to increase the interfacial contact area, Si is etched to form nanostructures such as nanowires, porous structures, periodic structures and quantum dots using techniques such as

chemical etching, reactive ion etching etc [11–14] . Nano structuring of Si results in increased surface area and significant decrease in the reflectivity due to increased light optical path.

However, surface nano structuring of Si results in some serious impediments such as a) enhanced electron-hole pair recombination due to high specific surface area, b) decrement in electrical conductivity due to quantum confinement effect and c) accelerated surface oxidation rates. To address the above-mentioned issues with the Si nanostructures, passivation layers or surface treatments are performed, which serve to decrease surface dangling bonds, trap states, surface states and control the parasitic carrier recombination rate. Lian et. al. demonstrated a interfacial engineered photodetector using PEDOT:PSS/Si heterojunction, where Si nanostructures are passivated with a methyl terminated surface groups (~CH_3), which resulted in a device performance of 37 mA/W.[15] Though passivation layers tend to enhance the device performance, they introduce particular challenges and limitations.[16] Inclusion of passivation layer increases the complexity of device fabrication process and also involves harmful organic solvents.

In this work, we demonstrate the fabrication of a high performance self-powered broadband photodetector employing hybrid heterojunction between Si nanostructures and PEDOT:PSS, without any additional passivation layer. Si nanoholes are fabricated using a metal assisted chemical etching technique and subsequently, the nanoholes are chemically polished to form nanotips, which result in the formation of a conformable junction with the PEDOT:PSS. To the best of authors knowledge, this is the first report demonstrating the chemical polishing-based passivation-free approach to boost the photoresponse of a self-powered photodetector.

2 Experimental

2.1 Materials

N-type Silicon wafer (100) with a resistivity of <10Ω and thickness 280 micron was procured from Aki Electronics. PEDOT:PSS and Silver Nitrate are procured from Sigma Aldrich. Sulfuric Acid, Hydrogen Peroxide, Nitric Acid and Ethylene Glycol were procured from FUJIFILM Wako Chemical Corporation.

2.2 Instrumentation

Reflectance was measured using an UV Vis spectrophotometer (Shimadzu UV-2450). Surface morphology and cross-section of the substrates were imaged using a scanning electron microscope (FE-SEM, Hitachi SU-8000). Device responsivity and External quantum efficiency were measured using a Spectral response measurement system (Bunkoukeiki BQE-100 F). Device transient photocurrent response at individual wavelengths was recorded using a Monochromator (Bunkoukeiki BSD-60Z), with a beam spot size of 2 cm^2. The irradiation intensity of the light sources was calibrated using a single-crystalline Si photodiode (Hamamatsu Photonics S1337–1010BQ). I-V characteristics of the devices were measured under an AM 1.5 simulated solar light from Xenon Arc lamp, with a beam size of 2 cm^2. Keithley 2400 semiconductor analyser was used to record the electrical measurements. Dark Current measurements were performed using a room temperature prober (Hisol HMP-400) coupled with a semiconductor analyser (Keithley 4000). Minority carrier lifetime of the samples was recorded using a carrier lifetime measurer (Sinton WCT-120). The active area of illumination in all the devices are maintained as 0.162 cm^2, using a mask.

2.3 Fabrication of Si nanostructures by metal assisted chemical etching and chemical polishing

Si nanostructures such as nanoholes and nanotips were fabricated by a two-step metal assisted chemical etching technique (MACE)[11–14] . Initially, the Si wafer (280 microns) was cleaned with acetone, DI water, Piranha solution, isopropanol, and water, under sonication for 10 minutes each. Silver ions were used as metal catalysts for the etching process. The cleaned wafers were immersed in a $AgNO_3$/HF solution for 5s, where the Ag ions get reduced over the surface of the Si wafer. The wafer with Ag ions was again, immersed in a HF/H_2O_2 solution for 30s, to preferentially remove the oxide layer present under the Ag ions and result in the formation of nanoholes. Further the Si wafers were immersed in a HNO_3 solution to remove the residual Ag particles and then subsequently treated in a diluted HF solution to remove the oxide formed during the etching process. Since the nanoholes offer poor infiltration for the PEDOT:PSS, the prepared nanohole samples were further chemically polished by immersing in a HNO_3/HF (40:1) etching solution for 5s-20s to form nanotips. Nanotips decrease the density of the nanostructures and thus offering enhanced infiltration for PEDOT:PSS. PEDOT:PSS solution is prepared by mixing the stock solution with isopropanol and ethylene glycol, which improves the infiltration and conductivity of the PEDOT:PSS. The diluted PEDOT:PSS was spin coated over the Si nanostructures at 4000 rpm for 60s and annealed at 140^{o}C for 10 minutes. For device fabrication, the Silver and Titanium, were deposited on rear side and finger patterned silver electrode was deposited on front side. Si nanostructure synthesis, PEDOT:PSS heterojunction formation and device fabrication is illustrated in **Figure 1.**

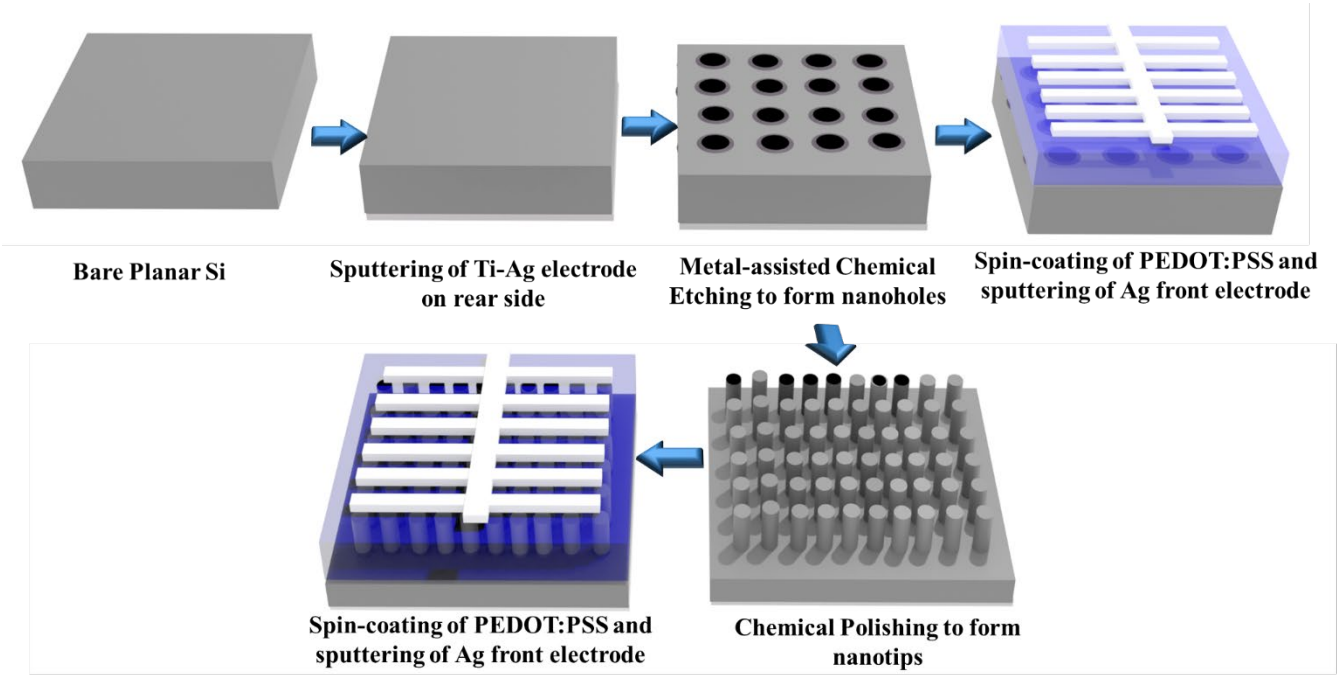

Figure 1. Si nanostructure synthesis by etching – polishing process and formation of junction with PEDOT:PSS for device fabrication

3 Results and discussion

3.1 Morphological Studies

FE-SEM images of Si substrates after metal-assisted chemical etching process and subsequent spin coating of PEDOT:PSS is shown in **Figure 2a**. Initially, substrate is immersed in a $AgNO_3$/HF solution for 5s. This immersion results in the oxidation of Si to Si di-oxide and subsequent reduction of Ag ion over the surface. Upon immersion in H_2O_2/HF solution for 30s, the Silicon dioxide underneath the Ag particle is rapidly dissolved to form dense nanostructures resulting in nanoholes. It is seen that roughly 500 nm-deep nanoholes were formed during the etching process. It is clearly visible from the image that the PEDOT:PSS layer is spread over the surface of nanoholes without any infiltration, which results in limited interfacial contact area between PEDOT:PSS and Si nanoholes. Thus, the performance of nanoholes device is

expected to be inferior owing to the poor infiltration. To alleviate this problem, an additional step of chemical polishing process is performed by immersing the nanoholes substrate in a HF/HNO_3 (1:40) solution to convert highly dense nanoholes to tapered nanotips. The nanohole samples are chemically polished for different timings from 5s to 20s. As seen in **Figure 2b**, polishing for 5s, the PEDOT:PSS infiltration inside the nanostructures has minimally increased, thus resulting improved contact between Si and PEDOT:PSS. Similarly, the polishing for 10s, further slightly increased the PEDOT:PSS infiltration (**Figure 2c**). Interestingly, with increased polishing time of 15s, the nanoholes are visibly tapered to form nanotips and the interfacial contact between the PEDOT:PSS and Si nanotips are very conformable (**Figure 2d**). For the sake of clarity, high magnification cross-sectional images of nanotips-15s sample are included in supplementary information (**Figure S1**). This results in a highly enhanced contact area between PEDOT:PSS and Si nanostructures. However, **Figure 2e** shows, with the further increase in polishing time to 20s, the nanotips seems to be tapered excessively, which is not desirable. Thus, we have obtained a highly conformable PEDOT:PSS/Si heterojunction by introducing an additional chemical polishing step and found optimized polishing duration of 15s.

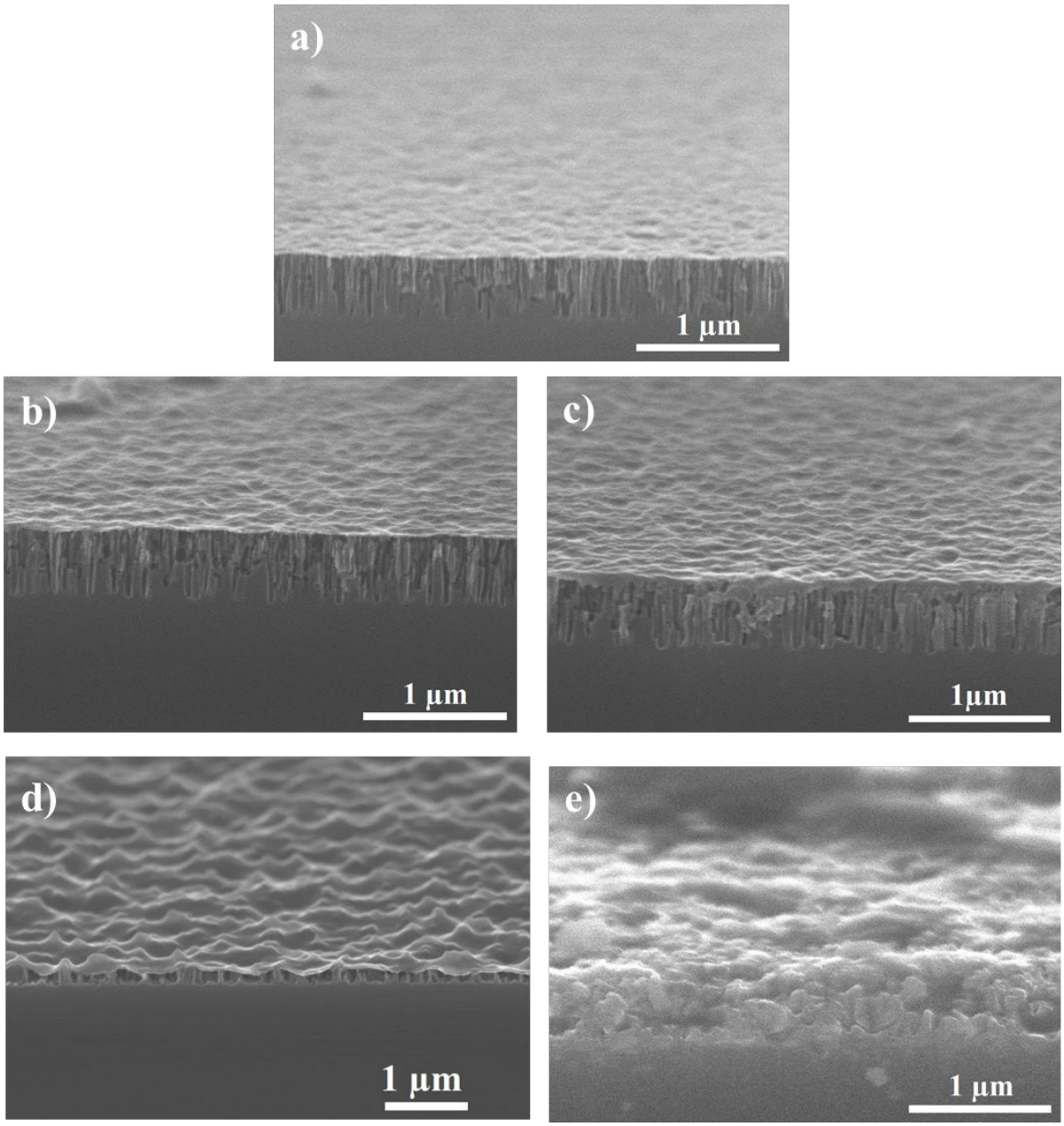

Figure 2. FE-SEM tilted cross-sectional images of a) nanoholes b) nanotips-5s c) nanotips-10s, d) nanotips-15s and e) nanotips-20s samples coated with PEDOT:PSS

3.2 Reflectance

Nano structuring of Si has profound effect on its optical properties. Hence, to probe the effect of etching on the optical characteristics of Si, the reflectance is measured. For the sake of reference, the reflectance of pristine planar Si is measured, as seen in **Figure 3a**. Surface roughness of the active layer significantly determines the light absorption characteristics in the device. Higher is the roughness of the layer, larger is the light trapping effect. Typically, pristine Si possess very low surface roughness, which results in the higher reflectance of the light. However, upon chemical etching process, surface roughness of the Si increases significantly, thus leading to decrease in the reflectance and enhanced light trapping effect. The planar Si has shown reflectance of around 40% in most of the measured spectral range, due to the smoother surface. Upon etching the reflectance of the Si substrates have drastically decreased to lesser than 10% over entire spectral range. As in the **Figure 3a**, nanoholes sample shows reflectance around 10% in 800 nm -1000 nm range and less than 5% in 350 nm – 800 nm. Further, it is to be noted that, with the chemical polishing process the reflectance has further reduced slightly lower than the nanohole samples. Lower reflectance in the etched Si nanostructured samples is due to the gradual change of refractive index at the surface.[17,18] The significant decrease in the reflectance after the chemical etching is attributed to the increased roughness, which is also seen in the SEM images (Figure 2). Thus, the reflectance studies reveal that the nano structuring of the Si has drastically decreased the reflectance of photons over wide spectral range. And, with the chemical polishing process, the reflectivity is further reduced slightly. Hence, the nanostructured Si is expected to boost the device performance owing to the enhanced light trapping effect.

I-V and Transient photocurrent response

To assess the device performance, testing is done under simulated light and monochromatic light conditions. As shown in the **Figure 3b** the device characteristics are studied by measuring

the I-V characteristics under simulated solar light with an intensity of 100 mW/cm^2. It is seen that all the fabricated detectors exhibit photo response to the white light. The nanoholes device has exhibited a short circuit current (I_{sc}) of 26.6 mA/cm^2. However, the chemically polished devices have exhibited enhanced short circuit current values of 27.97 mA/cm^2, 28.51 mA/cm^2, 31.18 mA/cm^2, and 30.51 mA/cm^2 for nanotips 5s, 10s, 15s and 20s samples, respectively. The device polished for 15s has shown the highest short circuit current density. As we have seen earlier in the SEM images (**Figure 2**), the nanohole sample has exhibited poor infiltration of PEDOT:PSS, resulting in limited interfacial contact area. And, upon chemically polishing, PEDOT:PSS infiltration was enhanced and the sample etched for 15s and 20s, has shown profound improvement in PEDOT:PSS infiltration. Thus, the short circuit current density of the devices, which reflect the device performance, seems to agree with the observations made in the FE-SEM images. Hence, it can be asserted that the PEDOT:PSS infiltration inside the Silicon nanostructures significantly affect the device performance. Further, the chemical polishing of the nanoholes to nanotips drastically improves the device performance, where the sample polished for 15s shows the best performance. It is also worth mentioning that, as we have seen in the **Figure 3a**, the reflectance of the samples have decreased with chemical polishing. Thus, the enhancement in device performance is also contributed by the decrease in reflectance due to the chemical polishing step.

Apart from the short circuit current density, fill factor and open-circuit voltage are also important parameters that are useful in assessing the performance of an opto-electronic device. High fill factor (FF) of a device indicates that the detector is effectively balancing the voltage and current outputs, resulting in a higher power output. The FF of a device is affected by the presence of unintended current paths (shunt resistance) and resistance in the electrical contacts (series resistance). [19,20] As we can see in the Figure 3a, the nanotips-5s sample seems to have the largest FF. Due to the short duration (5s) of chemical polishing, nanotips-5s sample is

expected to possess comparatively smoother surface morphology than other nanotips samples of longer duration. Thus, in the nanotips-5s sample, both the current pathways (shunt resistance) and contact resistance tend to be lower, which might have resulted in the higher FF. However, it is worth mentioning that, despite nanoholes also possessing smoother surface morphology, the FF is low. This can be attributed to the significantly high reflectance (**Figure 3a**) and poor light trapping by nanoholes.

Open-circuit voltage (V_{oc}) is the maximum voltage that can be extracted from the device, when the current through the device is zero. As we can see from the Figure 3b, the V_{oc} of nanoholes device is 0.35 V. However, with the chemical polishing process, the nanotips devices have shown increase in the Voc. Nanotips-5s and nanotips-10s devices have shown V_{oc} of 0.40 V and 0.42V, respectively. But, the nanotips-15s and nanotips-20s devices shown slight decrease in the V_{oc} to 0.38 V. V_{oc} is affected by the cumulative effect of factors such as energy gap of semiconductor, temperature, reverse saturation current and the presence of recombination centres. [21–23]

For power generating opto-electronic device such as solar cell, the I_{sc}, V_{oc}, and FF are collectively crucial in ensuring both sufficient current and voltage, to meet the specific requirements of the efficient power generation. However, in the context of a zero-bias operated photodetector, the I_{sc} is often more crucial than the V_{oc} and fill factor. In a photodetector, the magnitude of change in the device current upon light illumination is the key metric. I_{sc} is of primary importance because it determines the amount of electrical current that can be generated in the detector. In our case, the nanotips-15s device has shown the highest I_{sc}, which makes it the ideal for an efficient photodetector. Responsivity measurements (**Figure 3c**) also reveal that nanotips-15s sample shows highest photoresponsivity.

In comparison with the similar Si nanostructure/PEDOT:PSS heterojunction based photodetectors, our fabricated device shows superior performance. In a report based on Methyl

(~CH_3) passivated Si nanowires and PEDOT:PSS, the detector shows responsivity of 37 mA/W.[15] In another work, micro-nanostructure of porous Si (P-Si) is fabricated using etching and lithographic technique and formed heterojunction with PEDOT:PSS.[24] These P-Si micro nanostructures exhibit decent responsivity of 470 mA/W, however, fabrication process employed is complex and scalability is limited. Our fabricated optimized Si nanotips based device shows as an excellent responsivity of 555 mA/W at 0 V using a simpler device fabrication, without an extra passivation layer.

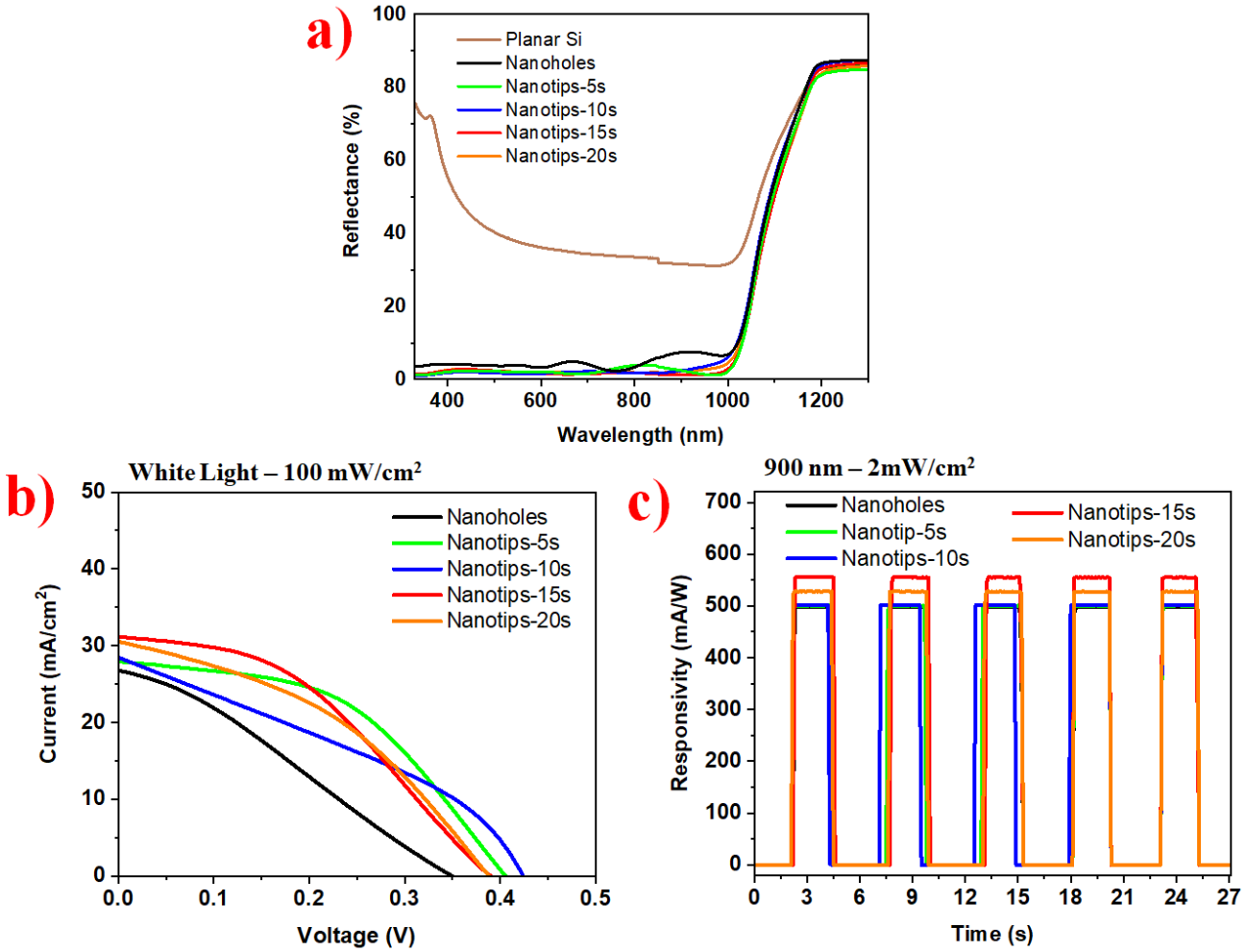

Figure 3. a) Reflectance of planar and nanostructured Si samples, b) I-V characteristics of the devices under solar simulator and c) Transient photo response of devices under monochromatic light (900 nm-2 mW/cm^2).

Further, to assess the device performance, transient photo response measurement is performed. Transient photo response analysis (TPA) is a technique employed to measure the magnitude of photocurrent generated in the device upon light illumination.[25] TPA also provides information related to how does the photocurrent in the device varies with time and how fast does the device respond to the photons, which are crucial for the assessment of photodetector devices. The transient photo response of all the devices was measured under a monochromatic light of wavelength 900 nm with an intensity of 2mW/cm^2. As the **Figure 3c** shows, all the fabricated devices respond to incident light, confirming the functioning of the device as a photodetector. The rise in the photocurrent is instantaneous and this reflects the ability of our device to function as a fast-response photodetector. The nanoholes device exhibited a responsivity of 498.35 mA/W. However, the chemically polished devices have exhibited enhanced responsivity values of 500.47 mA/W, 501.51 mA/W, 555.34 mA/W and 527.98 mA/W for nanotips 5s, 10s, 15s and 20s samples, respectively. Again, the transient photocurrent measurement confirms that the chemical polishing of the samples after etching, enhances the device performance.

To further analyse the exact phenomenon behind the enhanced device performance in the chemically polished samples, dark current and carrier lifetime measurements were performed. This was done to extract reverse saturation current density and carrier lifetime. I-V characteristics are measured under the dark conditions to study the charge transport and current-voltage relationship. Initially, to confirm the nature of the interfaces between Si and PEDOT:PSS with their electrodes, respective devices were fabricated and the I-V characteristics were studied. **Figures S2a and S2b** shows the I-V characteristics of Ti/Ag – Si – Ti/Ag device and Ag-PEDOT:PSS-Ag device, respectively. Both the fabricated devices showed linear I-V relation, which reveals the existence of ohmic transport mechanism and no energy barriers at the interfaces. **Figure 4a** shows the semi-logarithmic plots of I-V

characteristics under dark condition. It is seen that all the devices exhibit asymmetric I-V curves indicating the formation of a Schottky hybrid heterojunction between PEDOT:PSS and Si.[26,27] The measured I-V curves are fitted using ideal diode equation as per the thermionic emission model:

$$I = I_0 \left[\exp\left(\frac{qV}{nk_BT} \right) - 1 \right] \quad \text{--- Equation -1}$$

where q is electronic charge, V is voltage across the device, n is diode ideality factor, k_B is Boltzmann constant, T is absolute temperature, and I_o is reverse saturation current.

Reverse saturation current and diode-ideality factor were estimated using a linear fit to the straight-line segment of ln(I)-V plot.[28] Estimated reverse saturation current and diode ideality factors are plotted in the **Figure 4b**. Reverse saturation current values are found to be 6.3 µA, 0.69 µA, 3.42 µA, 0.42 µA, and 0.50 µA for nanoholes, nanotips-5s, nanotips-10s, nanotips-15s and nanotips-20s, respectively. Similarly, the diode ideality factor is estimated to be 2.38, 2.52, 2.49, 1.98 and 2.56 for nanoholes, nanotips-5s, nanotips-10s, nanotips-15s and nanotips-20s, respectively. The reverse saturation current (I_o) is a critical parameter in semiconductor diodes, which indicate the small and inherent current that flows through the diode under reverse biased conditions. Reverse saturation current is affected by the presence of defect and trap states in the diode. Larger is the defect density in the device, higher is the reverse saturation current. Hence, reverse saturation current serves as an indicator for the quality of the diode.[29] As seen in the **Figure 4b**, I_o has decreased by one order of magnitude after the chemical polishing process. This denote that the nanoholes sample has inherently larger defect density such as dangling bonds and surface states due to the etching process. Upon chemically polishing the nanoholes to nanotips, the defects are reduced due to the polishing process, which is reflected in the reverse saturation current.

Another device parameter, which also provides information regarding the defects, traps and recombination characteristics in the semiconductors is the minority carrier lifetime.[30,31] Transient photoconductivity (TPC) method is used to measure the minority carrier lifetime. TPC technique involves generating excess charge carriers in a semiconductor using a short pulse of LASER. The LASER illumination increases the conductivity in the material. The subsequent decay of the photogenerated carriers is monitored over the time. The rate at which the excess charge carriers recombine and photoconductivity decays infers about the minority carrier lifetime in the material. **Figure 4c** shows the measured minority carrier lifetime values in the plot. Minority carrier lifetime values are measured to be 38.21 µs, 39.27 µs, 39.53 µs, 51.18 µs and 45.32 µs for nanoholes, nanotips-5s, nanotips-10s, nanotips-15s and nanotips-20s samples, respectively. It is clearly seen that nanohole sample shows low carrier lifetime. The carrier lifetime has increased with the chemical polishing, as seen in the nanotips samples. This clearly validates that the process of chemical polishing defects states and thus improving the minority carrier lifetime.

Apart from the reduction of defects in the semiconductor, the chemical polishing process also leads to formation of a conformable heterojunction between the PEDOT:PSS and Si nanostructures as seen in the FE-SEM images (**Figure 1**). Hence, measurements such as dark I-V characteristics and carrier lifetime, reveal that the chemical polishing process improve the device performance by reducing the defect, trap states and paving way for fabrication of a conformable heterojunction. Especially, the nanotips-15s device has shown the superior performance among all. Hence, the nanotips-15s device is taken up for further photodetector performance testing.

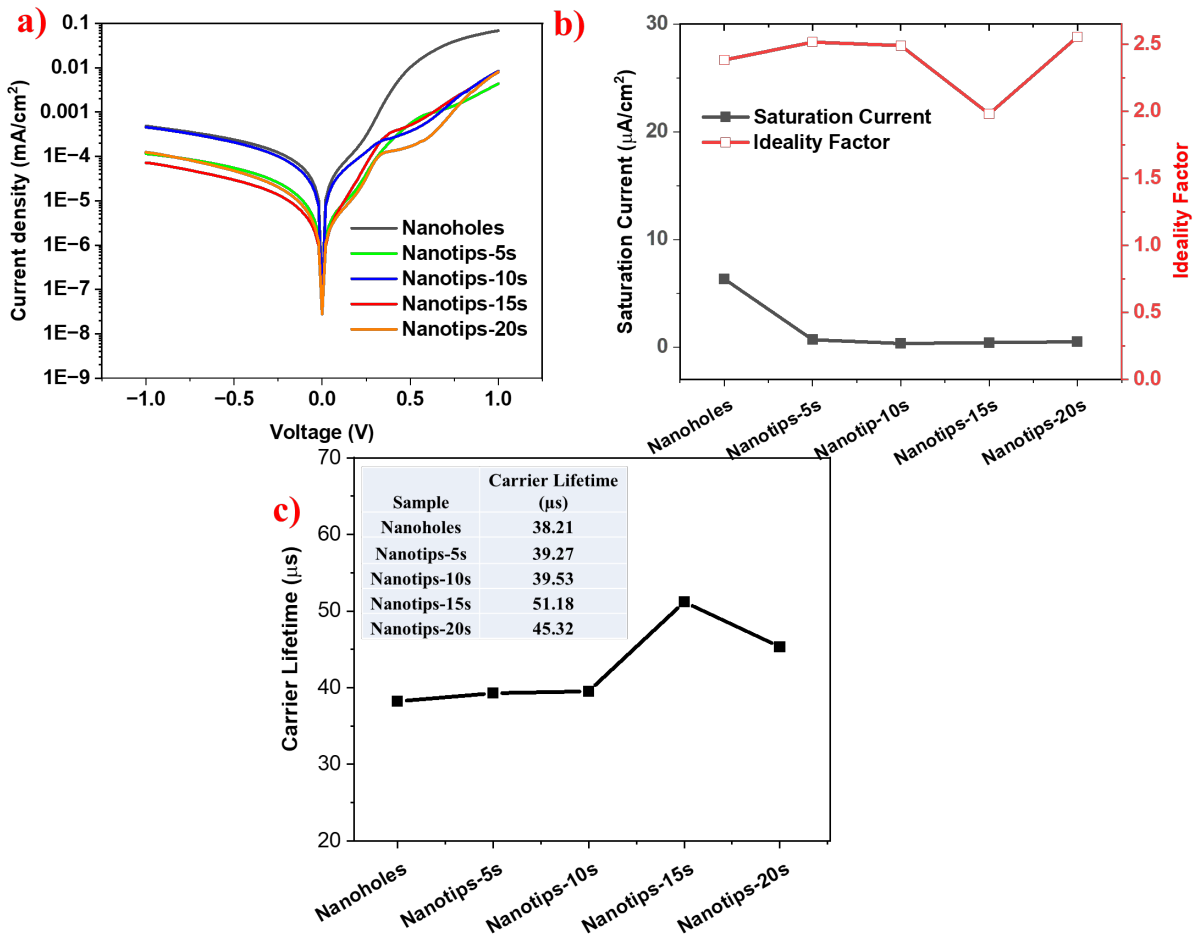

Figure 4. a) I-V characteristics of the devices under dark conditions. b) Estimated reverse saturation current density and diode ideality factor of the devices. c) Measured minority carrier lifetimes of the PEDOT:PSS/Si nanostructures.

3.3 Figures-of-merit

Figures-of-merit are the parameters which are useful for comparison of photodetectors with each other. Some of the key figures-of-merit are responsivity, external quantum efficiency and rise/fall time. Rise time is defined as the time taken for the device to 90% of its saturated photocurrent value from the 10% of the initial value.[32] Similarly, fall time is defined as the taken for the device to reach 90% of the dark current value from the 10% saturated photocurrent. Rise and fall time values indicate how fast does the photodetector respond to the incident photons.

Rise and fall times are estimated from the transient photoresponse response curve as seen in the **Figure 5a**. The device has exhibited a rise and fall times of 79 ms and 81 ms, respectively. The quicker rise/fall times of the detector demonstrates its potential for use in applications demanding fast response such as image recognition, spectroscopy etc.[33] Quicker rise and fall times of the detector is primarily attributed to the excellent crystallinity of the Si photoactive layer and hybrid junction between Si and PEDOT:PSS. Responsivity is defined as the ratio of photocurrent generated in the device to the photon intensity incident over the device per unit area. Responsivity indicates how efficiently the incident light intensity is being converted to photocurrent.[34] External quantum efficiency (EQE) is defined as the ratio of number of free charge carriers collected from the device to the number of photons incident on the device.[35] **Figure 5b** depicts the responsivity and EQE curves of the detector, which reveal that the detector demonstrate response over broad spectral range of photons from 400 nm to 1000 nm, which can be useful for broadband detection applications. The device exhibits a peak responsivity of around >550 mA/W in the range of 850 nm to 950 nm. Device also exhibits superior external quantum efficiency of around 0.8 over broad spectral range of 500 to 900 nm, which indicates that the incident photons are efficiently contributing to the free charge carrier generation and are being subsequently being collected at the electrodes. The superior figures-of-merit demonstrated by the detector is inherently attributed to the nano structuring of Silicon and the conformable junction between Si nanostructure and the PEDOT:PSS. The nano structuring of Si enhances the photon absorption due to the light trapping effect and leads to efficient charge carrier generation. The generated charge carriers are efficiently separated by the conformable PEDOT:PSS heterojunction and also transports the free charge carriers efficiently to the respective electrodes. As seen in the **Figure 3a**, after the chemical etching process, though the reflectance has decreased over wide spectral region covering 300-1000 nm, responsivity is minimal in the UV region (**Figure 5b**). Intrinsically, due to the narrower band

gap of the Si (1.1 eV), high energy photons (especially in UV range) generate hot carriers with excess energy, which resulting in heating up of crystal lattice, without any significant contribution to the photo response of the detector.[37] Further, the Si possess high UV absorption coefficient, thus the UV photons can penetrate only few nanometers and are absorbed within the shallow depth of Si.[36] Due to the absorption at the shallow depths, the recombination rate of photo generated carriers is relatively higher. These above-discussed phenomena contribute to the poor performance of Si photodetectors in the UV region.

Photocurrent of the detector with intensity varied from the 0.1 mW/cm^2 to 2 mW/cm^2 (900 nm) is measured to study the relation between photocurrent and light intensity, which reveals about the influence of defect states of the photoactive layers on the detector performance.[38,39] **Figure 5c** shows the intensity dependent transient photocurrent response of the device. The detector exhibits photocurrent values of 9.11 μA, 45.03, μA, 90.07 μA and 179.17 μA towards intensities of 0.1 mW/cm^2, 0.5 mW/cm^2, 1 mW/cm^2 and 2 mW/cm^2, respectively. The intensity dependent photocurrent values and corresponding responsivity values are plotted as shown in the **Figure 5d**. It is observed that the photocurrent varies linearly with the increase in the incident light intensity and the responsivity nearly remains similar at all the intensities. The linear relationship between incident photon intensity and the photocurrent indicates that the influence of defect states on the photocurrent generation seems to be insignificant.[40] The observed photocurrent linearity of the detector makes it suitable for applications which require high linear dynamic range such as intensity power meters, spectroscopy, ambient light detectors etc.

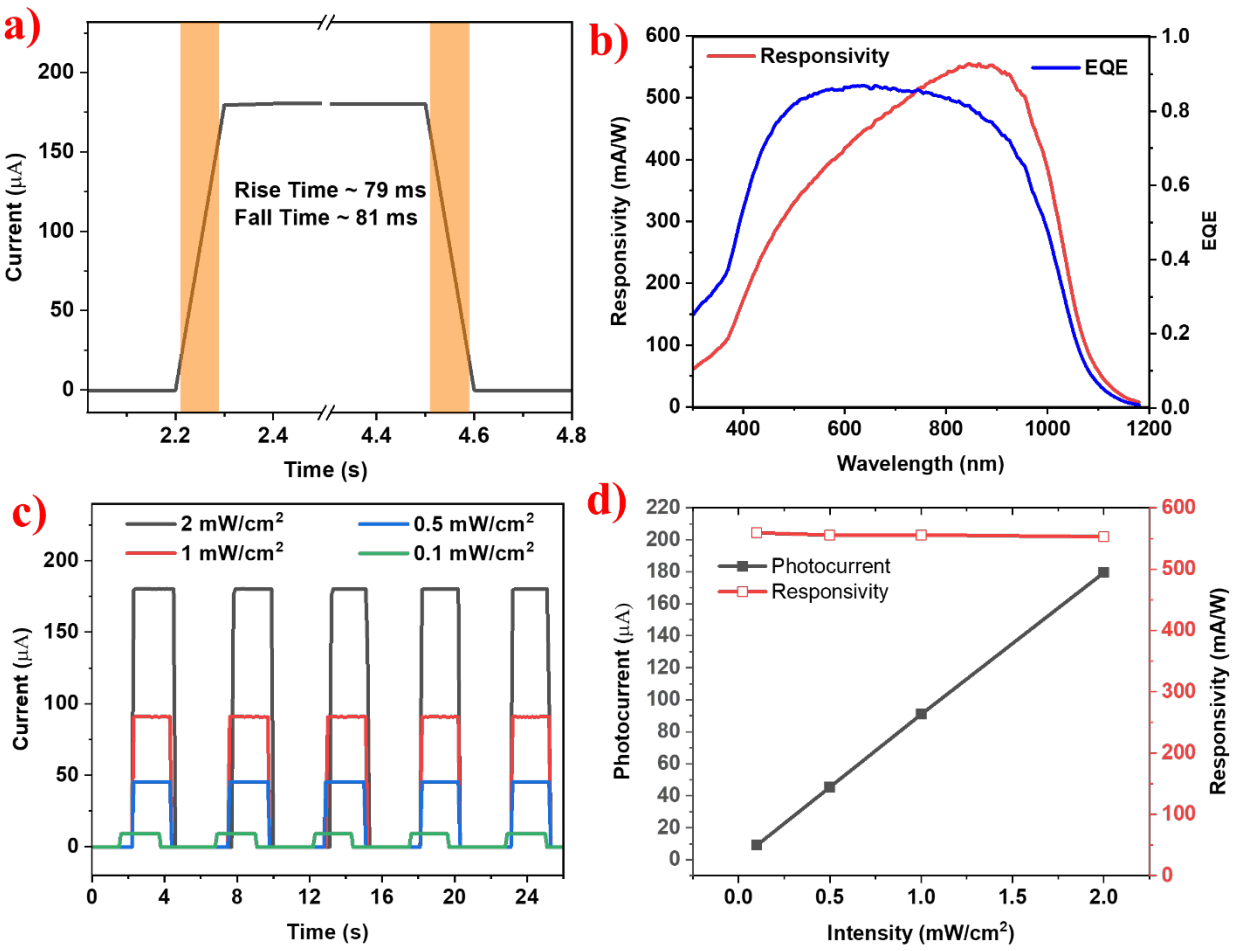

Figure 5. a) Rise / Fall time estimation, b) Responsivity and External quantum efficiency (EQE), c) Transient photo response under varied light intensities and d) Intensity dependent photocurrent and responsivity of nanotip-15s device.

3.4 Device Mechanism

To explain the process of heterojunction formation, photon absorption, charge carrier generation and charge transport, band diagram is illustrated as shown in the **Figure 6a.** PEDOT:PSS is a heavily doped p-type conducting polymer, which comprises of conducting PEDOT molecules dispersed using an insulating PSS molecules. PEDOT:PSS has high hole mobility and excellent visible light transparency, which makes it ideal as charge transport material for solar cells and photodetectors. Due to the quasi-metallic nature of PEDOT:PSS, the junction between PEDOT:PSS and n-type Si is often treated as Schottky junction in the

literature. Due to the p-type nature of the PEDOT:PSS, the Fermi level lies near the LUMO level. N-type Si is an indirect band gap semiconductor, with Fermi level lying near the conduction band. To physically form the heterojunction, PEDOT:PSS is spin coated onto the Si substrate. Upon the deposition, due to the Fermi level difference between the PEDOT:PSS and Si, the carriers start to flow from Si (high fermi level) to PEDOT:PSS (low Fermi level), until the charge carriers are equally distributed. Thus, the Fermi level lineup after reaching the equilibrium and results in the band bending at the interface, which denotes the generation of built-in field in the device. Under dark conditions, the current flowing through the device is very minimal. Under illuminated conditions, the photons are incident on the device from the top. Due to the highly transparent nature of the PEDOT:PSS, majority of the photons reach upto the Silicon and get absorbed at specific depth depending upon their absorption coefficient. High energy photons due to their higher absorption coefficient are absorbed near the top surface. Low energy photons, due to their poor absorption coefficient, are absorbed deep in the Silicon substrate. The absorbed photons generate free charge carriers in the Si and the charge carriers are readily transported to their respective electrodes readily due to the built-in in the device. The holes are collected by the PEDOT:PSS and the electrons reach the bottom Ti/Ag electrode due to the favourable band energetics. The transported free charge carriers are collected, which give rise to the photocurrent in the device. Due to the presence of built-in field, the device does not require any additional bias voltage, which makes it a self-powered photodetector. **Figure 6b** schematically illustrates the photon absorption, charge carrier generation and carrier collection in the device.

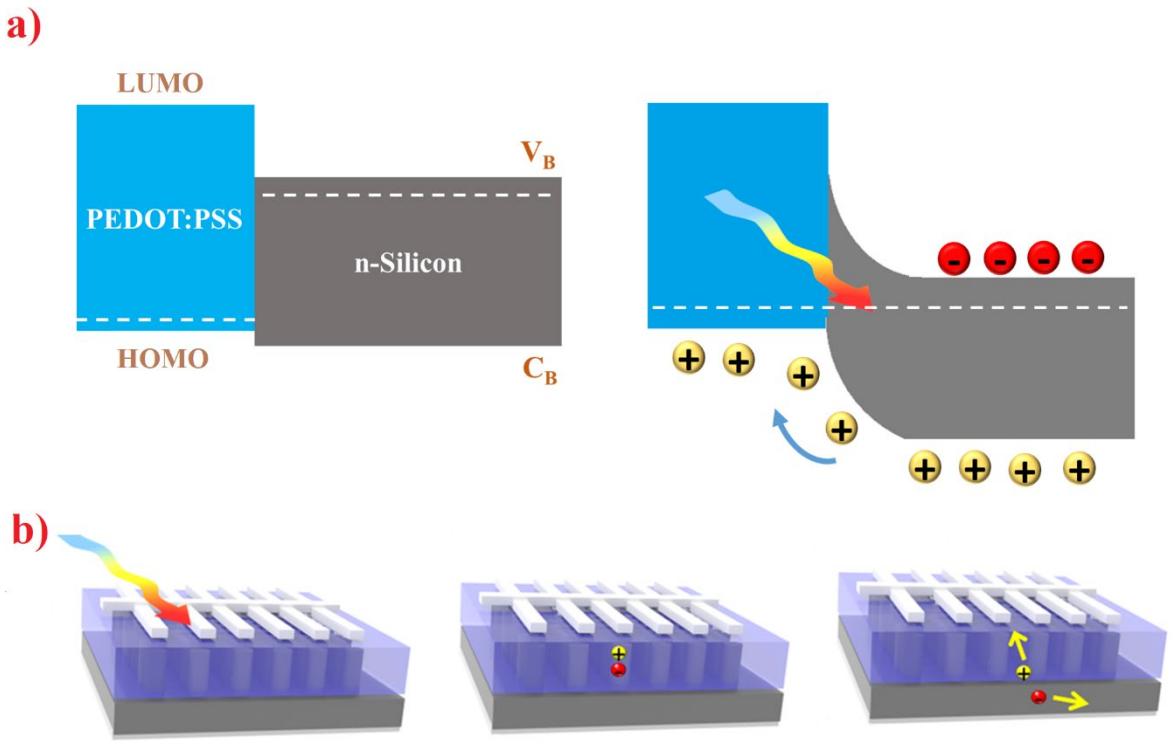

Figure 6. Schematic illustration of a) Heterojunction formation and band bending between Si and PEDOT:PSS, b) Photon absorption, charge generation and carrier transport process.

3.5 Cyclic Stability

For a photodetector to be useful for practical applications, the detector should possess high photostability. Photostability is the ability of the detector to retain its performance without any decrement, even after multiple cycles of photon illumination. Thus, to test the photostability of our fabricated photodetector, the device transient photocurrent analysis is performed, and responsivity is measured up to 500 illumination cycles. The device has exhibited a stable performance without significant difference from the initial throughout the entire testing photocycles, as seen in the **Figure S2**. This reveals that our fabricated detector possesses excellent photostability and can be used in applications where durability is required.

4. Comparison of the fabricated Si/PEDOT:PSS detector with similar class of photodetectors

In a report, Si nanowires are fabricated by metal assisted chemical etching technique and a conformable heterojunction is fabricated with PEDOT:PSS by tuning the spatial density of nanostructures.[15] Further, the nanowires are passivated with ~CH_3 group to reduce defects and improve the performance. Though, the device exhibited a quicker rise time of 2 μs, low responsivity of the detector is rather low (37 mA/W), despite the passivation. In another report, fabrication of Si microstructures based on porous-Si microarray is fabricated using an Electrochemical etching and lithographic technique is demonstrated.[24] Si- P-Si micro-nano structures are employed as a photodetector which exhibited a responsivity of 470 mA/W. Though the device has shown decent responsivity, the detector fabrication involves complex lithographic based approach which limits the scalability of the device. In another work, Si nanowires are fabricated using metal assisted chemical etching technique and are sensitized with hydrothermally-synthesized Graphene QDs.[44] Though, the device displays high responsivity of 25A/W due to photocarrier multiplication by Graphene quantum dots, the detector operates at higher bias voltage of 4V. Our work reports the fabrication of Si nanostructures by metal-assisted chemical etching technique and subsequent polishing process to reduce the surface defects. The chemical polishing process averts the requirement of passivation layer, thus simplifying the fabrication process. The fabricated Si nanostructures are formed conformable hybrid heterojunction with PEDOT:PSS and display excellent responsivity (555 mA/W), rise time (79 ms), EQE (0.8) and broad UV-Vis-NIR response at zero bias. Thus, our fabricated device shows superior performance in comparison with other photodetectors in literature in terms of responsivity as shown in Table 1.

Table 1. Comparison of our fabricated Si/PEDOT:PSS hybrid heterojunction photodetector with similar class of detectors.

Device Structure	Fabrication technique	Bias (V)	Responsivity	Rise Time	Ref
PEDOT:PSS/Si nanowire arrays	Metal assisted Chemical Etching (MACE)	0	37.8 mA/W (920)	2.03 µs	[15]
PEDOT:PSS/ Graphene	Exfoliation	0	162 mA/W (500 nm)	-	[41]
PEDOT:PSS/Ga_2O_3	MOCVD	0	37.4 mA/W (254 nm)	3.30 µs	[42]
PEDOT:PSS/(Si + PSi micro-arrays)	Electrochemical Etching	0	470 mA/W (900 nm)	396 µs	[24]
Si NW/Cs-$FAPbI_3$	MACE	0	14.86 mA/W (850 nm)	4 µs	[43]
PEDOT:PSS-Graphene QDs	MACE / Hydrothermal	4	25 A/W (750 nm)	79 ms	[44]
CdS-PEDOT:PSS	Chemical bath deposition	5	374 µA/W (NIR)	2.7 s	[32]
Si nanotips/PEDOT:PSS	MACE + Chemical polishing	0	555 mA/W	79 ms	This Work

5. Conclusions

The work demonstrates a passivation-free approach to enhance the performance of hybrid PEDOT:PSS/Si nanostructure based self-powered photodetector. Si nanostructures are fabricated by metal-assisted chemical etching technique. The fabricated Si nanostructures are subsequently chemically polished and heterojunction with PEDOT:PSS is fabricated by spin coating. It was found that the chemically polished samples exhibit improved PEDOT:PSS infiltration into Si nanostructures and formation of a conformable junction. The photodetector fabricated with chemically polished Si nanostructures demonstrated superior performance metrics such as high responsivity of 555.34 mA/W, quick rise/fall times of 79 / 81 ms and high EQE of 0.8 at zero bias (0V). Dark I-V characteristics and Carrier lifetime measurements were performed to study effect of chemical polishing on reverse saturation current and carrier lifetime. It is revealed that the chemical polishing has resulted in reduction of defects states, enhancement in carrier lifetime, formation of a conformable heterojunction in the device upon polishing.

Simple chemical polishing approach demonstrated, removes the need for passivation and thus would be beneficial for large scale fabrication of hybrid Si photodetectors.

Supporting information

High magnification FE-SEM images of nanotips-15s sample; Transient photo response of the fabricated detector under 500 illumination cycles to study the photostability.

CRediT authorship contribution statement

Kumaar Swamy Reddy B: Methodology, Investigation, Writing - original draft. Mostafa F. Abdelbar: Validation, Investigation, Writing – review & editing. Wipakorn Jevasuwan: Validation, Discussion, Writing - review & editing. Pramod H Borse: Investigation, Writing – review & editing. Sushmee Badhulika: Supervision, Investigation, Writing – review & editing. Naoki Fukata: Conceptualization, Resources, Writing - original draft, Supervision, Project administration, Funding acquisition.

Declaration of competing interest

The authors declare that they have no known competing financial interests or personal relationships that could have appeared to influence the work reported in this paper.

Data availability

The data supporting the findings of this study are available within this article and its supplementary information. Raw data that support the findings of this study area available from the authors, upon reasonable request.

REFERENCES

(1) Zhang, D.; Fuentes-Hernandez, C.; Vijayan, R.; Zhang, Y.; Li, Y.; Park, J. W.; Wang, Y.; Zhao, Y.; Arora, N.; Mirzazadeh, A.; Do, Y.; Cheng, T.; Swaminathan, S.; Starner, T.; Andrew, T. L.; Abowd, G. D. Flexible Computational Photodetectors for Self-Powered Activity Sensing. *Npj Flex. Electron.* **2022**, *6* (1), 1–8. https://doi.org/10.1038/s41528-022-00137-z.

(2) Nguyen, T. T.; Patel, M.; Kim, J. Self-Powered Transparent Photodetectors for Broadband Applications. *Surf. Interfaces* **2021**, *23*, 100934. https://doi.org/10.1016/j.surfin.2021.100934.

(3) *Highly flexible self-powered photodetectors based on core–shell Sb/CdS nanowires - Journal of Materials Chemistry C (RSC Publishing)*. https://pubs.rsc.org/en/content/articlelanding/2019/tc/c8tc06383d (accessed 2023-09-09).

(4) He, M.; Xu, Z.; Zhao, C.; Gao, Y.; Ke, K.; Liu, N.; Yao, X.; Kang, F.; Shen, Y.; Lin, L.; Wei, G. Sn-Based Self-Powered Ultrafast Perovskite Photodetectors with Highly Crystalline Order for Flexible Imaging Applications. *Adv. Funct. Mater.* **2023**, *33* (24), 2300282. https://doi.org/10.1002/adfm.202300282.

(5) Shiu, S.-C.; Chao, J.-J.; Hung, S.-C.; Yeh, C.-L.; Lin, C.-F. Morphology Dependence of Silicon Nanowire/Poly(3,4-Ethylenedioxythiophene):Poly(Styrenesulfonate) Heterojunction Solar Cells. *Chem. Mater.* **2010**, *22* (10), 3108–3113. https://doi.org/10.1021/cm100086x.

(6) Weickert, J.; Dunbar, R. B.; Hesse, H. C.; Wiedemann, W.; Schmidt-Mende, L. Nanostructured Organic and Hybrid Solar Cells. *Adv. Mater.* **2011**, *23* (16), 1810–1828. https://doi.org/10.1002/adma.201003991.

(7) Wright, M.; Uddin, A. Organic—Inorganic Hybrid Solar Cells: A Comparative Review. *Sol. Energy Mater. Sol. Cells* **2012**, *107*, 87–111. https://doi.org/10.1016/j.solmat.2012.07.006.

(8) Dutta, M.; Thirugnanam, L.; Trinh, P. V.; Fukata, N. High Efficiency Hybrid Solar Cells Using Nanocrystalline Si Quantum Dots and Si Nanowires. *ACS Nano* **2015**, *9* (7), 6891–6899. https://doi.org/10.1021/acsnano.5b03268.

(9) Fukata, N.; Subramani, T.; Jevasuwan, W.; Dutta, M.; Bando, Y. Functionalization of Silicon Nanostructures for Energy-Related Applications. *Small* **2017**, *13* (45), 1701713. https://doi.org/10.1002/smll.201701713.

(10) Subramani, T.; Chen, J.; Sun, Y.-L.; Jevasuwan, W.; Fukata, N. High-Efficiency Silicon Hybrid Solar Cells Employing Nanocrystalline Si Quantum Dots and Si Nanotips for Energy Management. *Nano Energy* **2017**, *35*, 154–160. https://doi.org/10.1016/j.nanoen.2017.03.037.

(11) Peng, K.-Q.; Yan, Y.-J.; Gao, S.-P.; Zhu, J. Synthesis of Large-Area Silicon Nanowire Arrays via Self-Assembling Nanoelectrochemistry. *Adv. Mater.* **2002**, *14* (16), 1164–1167. https://doi.org/10.1002/1521-4095(20020816)14:16<1164::AID-ADMA1164>3.0.CO;2-E.

(12) Huang, Z.; Geyer, N.; Werner, P.; de Boor, J.; Gösele, U. Metal-Assisted Chemical Etching of Silicon: A Review. *Adv. Mater.* **2011**, *23* (2), 285–308. https://doi.org/10.1002/adma.201001784.

(13) Jevasuwan, W.; Nakajima, K.; Sugimoto, Y.; Fukata, N. Metal-Catalyzed Electroless Etching and Nanoimprinting Silicon Nanowire-Based Solar Cells: Silicon Nanowire Defect Reduction and Efficiency Enhancement by Two-Step H2 Annealing. *Jpn. J. Appl. Phys.* **2016**, *55* (6), 065001. https://doi.org/10.7567/JJAP.55.065001.

(14) Chen, J.; Subramani, T.; Jevasuwan, W.; Dai, K.; Shinotsuka, K.; Hatta, Y.; Fukata, N. Fabrication of High-Performance Ordered Radial Junction Silicon Nanopencil Solar Cells by Fine-Tuning Surface Carrier Recombination and Structure Morphology. *Nano Energy* **2019**, *56*, 604–611. https://doi.org/10.1016/j.nanoen.2018.12.002.
(15) Liang, Z.; Zeng, P.; Liu, P.; Zhao, C.; Xie, W.; Mai, W. Interface Engineering To Boost Photoresponse Performance of Self-Powered, Broad-Bandwidth PEDOT:PSS/Si Heterojunction Photodetector. *ACS Appl. Mater. Interfaces* **2016**, *8* (29), 19158–19167. https://doi.org/10.1021/acsami.6b06301.
(16) Muduli, S. P.; Kale, P. State-of-the-Art Passivation Strategies of c-Si for Photovoltaic Applications: A Review. *Mater. Sci. Semicond. Process.* **2023**, *154*, 107202. https://doi.org/10.1016/j.mssp.2022.107202.
(17) Asadollahbaik, A.; Boden, S. A.; Charlton, M. D. B.; Payne, D. N. R.; Cox, S.; Bagnall, D. M. Reflectance Properties of Silicon Moth-Eyes in Response to Variations in Angle of Incidence, Polarisation and Azimuth Orientation. *Opt. Express* **2014**, *22* (102), A402–A415. https://doi.org/10.1364/OE.22.00A402.
(18) Bartschmid, T.; Wendisch, F. J.; Farhadi, A.; Bourret, G. R. Recent Advances in Structuring and Patterning Silicon Nanowire Arrays for Engineering Light Absorption in Three Dimensions. *ACS Appl. Energy Mater.* **2022**, *5* (5), 5307–5317. https://doi.org/10.1021/acsaem.1c02683.
(19) Qi, B.; Wang, J. Fill Factor in Organic Solar Cells. *Phys. Chem. Chem. Phys.* **2013**, *15* (23), 8972–8982. https://doi.org/10.1039/C3CP51383A.
(20) Wu, N.; Wu, Y.; Walter, D.; Shen, H.; Duong, T.; Grant, D.; Barugkin, C.; Fu, X.; Peng, J.; White, T.; Catchpole, K.; Weber, K. Identifying the Cause of Voltage and Fill Factor Losses in Perovskite Solar Cells by Using Luminescence Measurements. *Energy Technol.* **2017**, *5* (10), 1827–1835. https://doi.org/10.1002/ente.201700374.
(21) Jeong, M. S.; Min, K. H.; Choi, S.; Kang, M. G.; Jeong, K. T.; Lee, E. T.; Kang, Y.; Kim, D.; Lee, H.-S.; Song, H.; Park, S. Correlation between the Open-Circuit Voltage and Recombination Loss at Metal-Silicon Interfaces of Crystalline Silicon Solar Cells. *Sol. Energy Mater. Sol. Cells* **2020**, *210*, 110519. https://doi.org/10.1016/j.solmat.2020.110519.
(22) *Limits on the open-circuit voltage and efficiency of silicon solar cells imposed by intrinsic Auger processes*. https://ieeexplore.ieee.org/document/1483873 (accessed 2023-11-10).
(23) Daboczi, M.; Hamilton, I.; Xu, S.; Luke, J.; Limbu, S.; Lee, J.; McLachlan, M. A.; Lee, K.; Durrant, J. R.; Baikie, I. D.; Kim, J.-S. Origin of Open-Circuit Voltage Losses in Perovskite Solar Cells Investigated by Surface Photovoltage Measurement. *ACS Appl. Mater. Interfaces* **2019**, *11* (50), 46808–46817. https://doi.org/10.1021/acsami.9b16394.
(24) Ramadan, R.; Torres-Costa, V.; Martín-Palma, R. J. Self-Powered Broadband Hybrid Organic–Inorganic Photodetectors Based on PEDOT:PSS and Silicon Micro-Nanostructures. *J. Mater. Chem. C* **2021**, *9* (13), 4682–4694. https://doi.org/10.1039/D1TC00329A.
(25) *Transient photocurrent response of three-color detectors based on amorphous silicon - Google Search*. https://www.google.com/search?client=firefox-b-d&q=Transient+photocurrent+response+of+three-color+detectors+based+on+amorphous+silicon (accessed 2023-09-12).
(26) Jäckle, S.; Mattiza, M.; Liebhaber, M.; Brönstrup, G.; Rommel, M.; Lips, K.; Christiansen, S. Junction Formation and Current Transport Mechanisms in Hybrid N-Si/PEDOT:PSS Solar Cells. *Sci. Rep.* **2015**, *5* (1), 13008. https://doi.org/10.1038/srep13008.
(27) Javadi, M.; Mazaheri, A.; Torbatiyan, H.; Abdi, Y. Mechanism of Charge Transport in Hybrid Organic-Inorganic PEDOT:PSS/Silicon Heterojunctions. *Phys. Rev. Appl.* **2019**, *12* (3), 034002. https://doi.org/10.1103/PhysRevApplied.12.034002.

(28) Abdelhameed, M.; Abdelbar, M. F.; El Basaty, A. B.; Jevasuwan, W.; Dai, K.; Shinotsuka, K.; Hatta, Y.; Fukata, N. Current Transport Characterization and Photovoltaic Performance of Si Nanopencil-Based Schottky Junction Assisted with VOx as a Hole-Injection Layer. *Micro Nanostructures* **2023**, *176*, 207519. https://doi.org/10.1016/j.micrna.2023.207519.
(29) Singh, P.; Ravindra, N. M. Temperature Dependence of Solar Cell Performance—an Analysis. *Sol. Energy Mater. Sol. Cells* **2012**, *101*, 36–45. https://doi.org/10.1016/j.solmat.2012.02.019.
(30) Murphy, J. D.; McGuire, R. E.; Bothe, K.; Voronkov, V. V.; Falster, R. J. Minority Carrier Lifetime in Silicon Photovoltaics: The Effect of Oxygen Precipitation. *Sol. Energy Mater. Sol. Cells* **2014**, *120*, 402–411. https://doi.org/10.1016/j.solmat.2013.06.018.
(31) Shah, D. K.; Kc, D.; Kim, T.-G.; Akhtar, M. S.; Kim, C. Y.; Yang, O.-B. Influence of Minority Charge Carrier Lifetime and Concentration on Crystalline Silicon Solar Cells Based on Double Antireflection Coating: A Simulation Study. *Opt. Mater.* **2021**, *121*, 111500. https://doi.org/10.1016/j.optmat.2021.111500.
(32) Reddy B, K. S.; Veeralingam, S.; Borse, P. H.; Badhulika, S. Synchronous Enhancement of Responsivity, Response Time and, Spectral Range in Solution Processed CdS Photodetector upon Modification with PEDOT:PSS. *J. Alloys Compd.* **2022**, *919*, 165775. https://doi.org/10.1016/j.jallcom.2022.165775.
(33) Yun, K.-R.; Lee, T.-J.; Kim, S.-K.; Kim, J.-H.; Seong, T.-Y. Fast and Highly Sensitive Photodetectors Based on Pb-Free Sn-Based Perovskite with Additive Engineering. *Adv. Opt. Mater.* **2023**, *11* (1), 2201974. https://doi.org/10.1002/adom.202201974.
(34) Reddy, B. K. S.; Veeralingam, S.; Borse, P. H.; Badhulika, S. A Flexible, Rapid Response, Hybrid Inorganic–Organic SnSe2–PEDOT:PSS Bulk Heterojunction Based High-Performance Broadband Photodetector. *Mater. Chem. Front.* **2022**, *6* (3), 341–351. https://doi.org/10.1039/D1QM01232K.
(35) Reddy, K. S. B.; Panda, S.; Ramasamy, E.; Veerappan, G.; Badhulika, S.; Borse, P. H. Fabrication of Self-Powered Broadband Photodetector by 50% Replacement of Pb by Mg in CH3NH3Pb0.5Mg0.5Cl2I Perovskite Lattice. *Mater. Adv.* **2023**. https://doi.org/10.1039/D3MA00411B.
(36) Wolffenbuttel, R. F. Photodiodes in Silicon with an Electrically-Programmable UV Response. *Sens. Actuators Phys.* **1990**, *22* (1), 559–563. https://doi.org/10.1016/0924-4247(89)80035-4.
(37) Sinha, A.; Qian, J.; Moffitt, S. L.; Hurst, K.; Terwilliger, K.; Miller, D. C.; Schelhas, L. T.; Hacke, P. UV-Induced Degradation of High-Efficiency Silicon PV Modules with Different Cell Architectures. *Prog. Photovolt. Res. Appl.* **2023**, *31* (1), 36–51. https://doi.org/10.1002/pip.3606.
(38) Huang, S.-M.; Lin, L.-J.; Yan, Y.-J.; Yu, S.-H.; Chou, M. M. C.; Hsieh, H.-F.; Ho, C.-J.; Chen, R.-S. The Extremely Enhanced Photocurrent Response in Topological Insulator Nanosheets with High Conductance. *Nanoscale Res. Lett.* **2018**, *13* (1), 371. https://doi.org/10.1186/s11671-018-2758-0.
(39) Wang, Y.; Zhang, Y.; Lu, Y.; Xu, W.; Mu, H.; Chen, C.; Qiao, H.; Song, J.; Li, S.; Sun, B.; Cheng, Y.-B.; Bao, Q. Hybrid Graphene–Perovskite Phototransistors with Ultrahigh Responsivity and Gain. *Adv. Opt. Mater.* **2015**, *3* (10), 1389–1396. https://doi.org/10.1002/adom.201500150.
(40) Bao, C.; Chen, Z.; Fang, Y.; Wei, H.; Deng, Y.; Xiao, X.; Li, L.; Huang, J. Low-Noise and Large-Linear-Dynamic-Range Photodetectors Based on Hybrid-Perovskite Thin-Single-Crystals. *Adv. Mater.* **2017**, *29* (39), 1703209. https://doi.org/10.1002/adma.201703209.

(41) Liu, Z.; Parvez, K.; Li, R.; Dong, R.; Feng, X.; Müllen, K. Transparent Conductive Electrodes from Graphene/PEDOT:PSS Hybrid Inks for Ultrathin Organic Photodetectors. *Adv. Mater.* **2015**, *27* (4), 669–675. https://doi.org/10.1002/adma.201403826.
(42) Li, S.; Yan, Z.; Liu, Z.; Chen, J.; Zhi, Y.; Guo, D.; Li, P.; Wu, Z.; Tang, W. A Self-Powered Solar-Blind Photodetector with Large Voc Enhancing Performance Based on the PEDOT:PSS/Ga2O3 Organic–Inorganic Hybrid Heterojunction. *J. Mater. Chem. C* **2020**, *8* (4), 1292–1300. https://doi.org/10.1039/C9TC06011A.
(43) Liu, J.-Q.; Gao, Y.; Wu, G.-A.; Tong, X.-W.; Xie, C.; Luo, L.-B.; Liang, L.; Wu, Y.-C. Silicon/Perovskite Core–Shell Heterojunctions with Light-Trapping Effect for Sensitive Self-Driven Near-Infrared Photodetectors. *ACS Appl. Mater. Interfaces* **2018**, *10* (33), 27850–27857. https://doi.org/10.1021/acsami.8b08387.
(44) *Engineering Graphene Quantum Dots for Enhanced Ultraviolet and Visible Light p-Si Nanowire-Based Photodetector | ACS Applied Materials & Interfaces*. https://pubs.acs.org/doi/10.1021/acsami.7b07667 (accessed 2023-09-09).